Fourier Analysis To Measure Diffusion Coefficients and Resolve Mixtures on a Continuous Electrophoresis Chip

8 AUTHORS, INCLUDING:

Vincent Croquette

French National Centre for Scientific Research

123 PUBLICATIONS **7,706** CITATIONS

SEE PROFILE

Annie Lemarchand

French National Centre for Scientific Research

101 PUBLICATIONS **721** CITATIONS

SEE PROFILE

Ludovic Jullien

Ecole Normale Supérieure de Paris

137 PUBLICATIONS **3,023** CITATIONS

SEE PROFILE

Fourier Analysis To Measure Diffusion Coefficients and Resolve Mixtures on a Continuous Electrophoresis Chip

A. Estévez-Torres,[†] C. Gosse,*,[‡] T. Le Saux,[†] J.-F. Allemand,[§] V. Croquette,[§] H. Berthoumieux,[†] A. Lemarchand,[‖] and L. Jullien*,[†]

Ecole Normale Supérieure, Département de Chimie, UMR CNRS ENS Université Paris6 8640, 24, rue Lhomond, 75005 Paris, France, Laboratoire de Photonique et de Nanostructures, LPN-CNRS, Route de Nozay, 91460 Marcoussis, France, Ecole Normale Supérieure, Département de Physique, UMR CNRS ENS Université Paris6 and Paris7 8550, 24, rue Lhomond, 75005 Paris, France, and Laboratoire de Physique Théorique de la Matiere Condensée, Université Pierre et Marie Curie Paris 6, UMR CNRS 7600, 4, place Jussieu, 75252 Paris Cedex 05, France

We report a method to measure diffusion coefficients of fluorescent solutes in the 10^2−10^6 Da molecular mass range in a glass−PDMS chip. Upon applying a permanent electric field, the solute is introduced through a narrow channel into a wide analysis chamber where it migrates along the injection axis and diffuses in two dimensions. The diffusion coefficient is extracted after 1D Fourier transform of the resulting stationary concentration pattern. Analysis is straightforward, requiring no numerical integration or velocity field simulation. The diffusion coefficients measured for fluorescein, rhodamine green-labeled oligonucleotides, and YOYO-1-stained dsDNA fragments agree with the literature values and with our own fluorescence correlation spectroscopy measurements. As shown for 151 and 1257 base pair dsDNA mixtures, the present method allows us to rely on diffusion to quantitatively characterize the nature and the composition of binary mixtures. In particular, we implement a DNA hybridization assay to illustrate the efficiency of the proposed protocol for library screening.

Phenomenologically expressing the friction with the medium, the molecular diffusion coefficient D depends on the size, the shape, and the charge distribution of the considered species.[1] However, despite its specificity, diffusion has not drawn much attention in the context of analysis. Indeed, D is not markedly sensitive to the detailed structure of molecules sharing a similar size. Consequently, the analysis of the diffusive behavior is generally not appropriate to study samples with numerous unknown components. Nevertheless, diffusion can efficiently discriminate two mixture components that significantly differ by their size, typically at least by a factor of 2. In fact, the latter situation is often relevant in titrations of pharmaceutical or

biological interest where one wants to access the relative proportions in two states of a ligand: free or bound to a large protein target. Measurements of diffusion coefficients relying on either NMR spectroscopy[2] or fluorescence emission[3,4] have been applied to library screening and lead identification. Moreover, an immunoassay relying on reagents mixing by diffusion has been developed to titrate small drug molecules in whole blood samples.[5] In this analytical context, Brownian motion is a particularly attractive process with respect to throughput and miniaturization. Indeed, a nanometer-size molecule in a typical liquid at room temperature has a diffusion coefficient in the few 10^{-10} M^{-1} s^{-1} range, thus allowing D to be extracted in 1 s by observing molecular motion at the 20-μm scale.

Among the many methods available to measure diffusion coefficients,[6−12] those requiring low sample amounts have to be favored when working with scarce biological material. From this point of view, techniques based on fluorescence emission are particularly attractive, allowing for measurements down to nanomolar concentrations.[9,10] Implemented, for instance, in fluorescence correlation spectroscopy (FCS), a first approach relies on observing the density fluctuations in an open volume containing a few molecules. Although powerful, this technique is intrinsically limited by its low concentration requirement, which hinders D extraction except for strongly fluorescent substrates. One may thus prefer a second and more macroscopic approach based on the temporal relaxation analysis of an out-of-equilibrium concentration profile. For example, in fluorescence recovery after

---

* To whom correspondence should be addressed. E-mail: Ludovic.Jullien@ens.fr; charlie.gosse@lpn.cnrs.fr.
  † Département de Chimie, UMR CNRS ENS Université Paris6.
  ‡ Laboratoire de Photonique et de Nanostructures.
  § Département de Physique, UMR CNRS ENS Université Paris6 and Paris7.
  ‖ Université Pierre et Marie Curie Paris 6.

(1) Cantor, C. R.; Schimmel, P. R. *Biophysical Chemistry,* Part II; Freeman: New York, 1980.
(2) Chen, A.; Shapiro, M. J. *Anal. Chem.* **1999,** *71,* 669A−675A.
(3) Auer, M.; Moore, K. J.; Meyer-Almes, F. J.; Guenther, R.; Pope, A. J.; Stoeckli, K. A. *Drug Discovery Today* **1998,** *3,* 457−465.
(4) Kaufman, E. N.; Jain, R. K. *J. Immunol. Methods* **1992,** *155,* 1−17.
(5) Hatch, A.; Kamholz, A. E.; Hawkins, K. R.; Munson, M. S.; Schilling, E. A.; Weigl, B. H.; Yager, P. *Nat. Biotechnol.* **2001,** *19,* 461−465.
(6) Taylor, G. *Proc. R. Soc. London, Ser. A* **1953,** *219,* 186−203.
(7) Culbertson, C.T.; Jacobson, S.C.; Ramsey, J.M. *Talanta* **2002,** *56,* 365−373.
(8) Stilbs, P. *Anal. Chem.* **1981,** *53,* 2135−2137.
(9) Elson E. L. *Annu. Rev. Phys. Chem.* **1985,** *36,* 379−406.
(10) Sprague, B. L.; McNally, J. G. *Trends Cell. Biol.* **2005,** *15,* 84−91.
(11) Schurr, J. M. *CRC Crit. Rev. Biochem.* **1977,** *4,* 371−431.
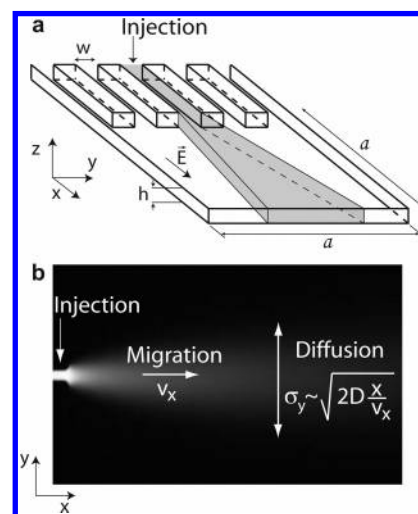(12) Zhang, K. J.; Briggs, M. E.; Gammon, R. W.; Sengers; J. V. *J. Chem. Phys.* **1996,** *104,* 6881−6892.

photobleaching (FRAP), a light source of tunable power is used both to create the initial out-of-equilibrium condition and to read out the temporal evolution of the system. More recently, microfluidic devices have been used instead of photolysis to generate various out-of-equilibrium concentration profiles:[13−15] their geometry is compatible with epifluorescence microscopy and they only require minute sample amounts. In the T-sensor for instance,[13,16] two reactive solutions are injected at constant rate into the arms of either T- or Y-shaped microchannels. Under conditions of strictly laminar and permanent flow, mixing is only governed by diffusion−reaction processes and the analysis of the concentration profile of the fluorescent solute along the channel may provide diffusion coefficients[13,16,17] and rate constants.[13,17]

In spite of the T-sensor design simplicity, the parabolic velocity profile generated by pressure-driven flows considerably complicates the reliable derivation of molecular parameters.[18−20] In particular, for each channel geometry and each flow rate, an accurate estimation of mass transport has to be performed to avoid artifacts.[21] In the present account, we introduce an alternative device for measuring diffusion coefficients. One here analyzes the electric field-generated migration−diffusion pattern of fluorescent species, which are introduced into a microfabricated chamber using a narrow channel. As in a T-sensor, the concentration profiles are stationary, making signal integration possible in the case of dilute or poorly fluorescent solutes. However, the electric field-generated velocity profile is now pluglike and constant over the entire analysis area. Therefore, an exact analytic solution for the migration−diffusion pattern can be derived.

The stationary migration−diffusion pattern observed in our device is not a simple function of the space coordinates and the D derivation directly from the recorded image would be difficult. We alternatively considered analyzing the experimental data in the Fourier space in which the extraction of the diffusion coefficients is easy and requires no numerical integration. Such a strategy has already been implemented to measure diffusion coefficients in FRAP experiments.[22,23] However, Fourier transform has been rarely used to analyze diffusion or dispersion phenomena in 1D separations. Indeed, the analysis of the temporal broadening of a Gaussian peak remains the preferred approach.[7]

The paper is organized as follows. In the second section, we introduce the theoretical model subsequently used to extract the diffusion coefficients from the experimental data. The third section is devoted to the experimental part. In particular, we here characterize the microdevice features. The results and the corresponding discussion are given in the fourth section. We show that the diffusive behavior within the measurement chamber can

(13) Kamholz, A. E.; Weigl, B. H.; Finlayson, B. A.; Yager, P. *Anal. Chem.* **1999**, *71*, 5340−5347.
(14) Dertinger, S. K. W.; Chiu, D. T.; Jeon, N. L.; Whitesides, G. M. *Anal. Chem.* **2001**, *73*, 1240−1246.
(15) Cabrera, C. R.; Finlayson, B.; Yager, P. *Anal. Chem.* **2001**, *73*, 658−666.
(16) Kamholz, A. E.; Schilling, E. A.; Yager, P. *Biophys. J.* **2001**, *80*, 1967−1972.
(17) Salmon, J.-B.; Dubrocq, C.; Tabeling, P.; Charier, S.; Alcor, D.; Jullien, L.; Ferrage, F. *Anal. Chem.* **2005**, *77*, 3417−3424.
(18) Ismagilov, R. F.; Stroock, A. D.; Kenis, P. J. A.; Whitesides, G. *Appl. Phys. Lett.* **2000**, *76*, 2376−2378.
(19) Beard, D. A. *J. Appl. Phys.* **2001**, *89*, 4667−4669.
(20) Kamholz, A. E.; Yager, P. *Biophys. J.* **2001**, *80*, 155−160.
(21) Salmon, J.-B.; Ajdari, A. *J. Appl. Phys.* **2007**, *101*, 074902.
(22) Tsay, T.-T.; Jacobson, K. A. *Biophys. J.* **1991**, *60*, 360−368.
(23) Berk, D. A.; Yuan, F.; Leunig, M.; Jain, R. K. *Biophys. J.* **1993**, *65*, 2428−2436.

Figure 1. Principle of the measurement of a diffusion coefficient in a continuous electrophoresis chip. (a) The application of a voltage drop along the x axis yields the sample introduction from a narrow ($w = 20$ μm) and thin ($h = 10$ μm) injection channel, into a wide ($a = 7.5$ mm) square analysis chamber. (b) In the zone where the electric field $\vec{E}$ is uniform and parallel to the x axis, $\vec{E} = E_x\vec{u}_x$, the solute **F** migrates at constant velocity v_x. After a transient regime, a stationary parabola-like migration−diffusion pattern is established with a typical width $\sigma_y \sim (2Dx/v_x)^{1/2}$ at abscissa x. In the present work, this migration−diffusion pattern is subsequently analyzed by spatial Fourier transform along y to provide the diffusion coefficient D after v_x measurement.

be fruitfully investigated by 1D Fourier transform analysis to yield accurate values of diffusion coefficients. We also address the issue of analyzing a binary mixture by observing the migration−diffusion process of its components. The conclusion is provided in the last section.

THEORY

Figure 1 displays the principle of the present stationary approach to measure the diffusion coefficient of a fluorescent analyte **F**. Experiments are performed in a 10-μm thin microsystem where the **F** solution is in contact, through a 20-μm narrow channel, with a 7.5-mm-wide square chamber filled with the migration medium (Figure 1a). Application of a permanent electric potential drop along the channel axis, i.e., the x one, results in continuous solute injection into the chamber: After a transient regime, a stationary migration−diffusion pattern is obtained (Figure 1b). Provided that the **F** velocity within the chamber can be measured, the analysis of this pattern yields the **F** diffusion coefficient.

To calculate analytically the stationary migration−diffusion pattern of **F**, we consider the motion to occur in a 2D medium[24] defined by $0 \leq x \leq a$ and $-\infty < y < +\infty$. This medium is submitted to a uniform and permanent electric field $\vec{E} = E_x\vec{u}_x$ with $\vec{u}_x$ the unit vector along x. Species **F** migrates in the direction of increasing x with a velocity v_x and diffuses along x and y with a molecular diffusion coefficient D. The velocity field of the **F** analyte is uniform and parallel to the x axis only beyond a characteristic

(24) The velocity field of the species **F** can be essentially considered as constant along z in the whole device (vide infra). As the **F** concentration at the injection point is also independent on z, the problem is rigorously bidimensional.

distance l_0 from the injection nozzle (vide infra); we thus set the x origin at this point and restrict the following theoretical analysis to the downstream area.

In the absence of any dispersive contributions, the stationary concentration profile $F(x,y)$ obeys the partial differential equation:

$$-v_x \frac{\partial F(x, y)}{\partial x} + D\left[\frac{\partial^2 F(x,y)}{\partial x^2} + \frac{\partial^2 F(x, y)}{\partial y^2}\right] = 0 \qquad (1)$$

where the first term originates from $\mathbf{F}$ migration and the second term from $\mathbf{F}$ diffusion. Admitting that the concentration profiles are fixed at $x = 0$ and $x = a$, $F(0, y)$ and $F(a, y)$ can correspondingly be used as boundary conditions.

The calculation of the migration−diffusion concentration pattern is much easier in the Fourier space. Thus, we look for an expression of the Fourier transform of the concentration $F(x,y)$ with respect to y: $\tilde{F}(x, q) = 1/(2\pi)^{1/2} \int_{-\infty}^{\infty} F(x, y) e^{-iqy} \, \mathrm{d}y$. Equation 1 yields

$$\frac{\partial^2 \tilde{F}(x, q)}{\partial x^2} - \frac{v_x}{D} \frac{\partial \tilde{F}(x, q)}{\partial x} - q^2 \tilde{F}(x, q) = 0 \qquad (2)$$

The general solution of the preceding equation reads

$$\tilde{F}(x, q) = C_- \exp(\lambda_- x) + C_+ \exp(\lambda_+ x) \qquad (3)$$

where the eigenvalues obey

$$\lambda_\pm = \frac{1 \pm \sqrt{1 + 4D^2 q^2/v_x^2}}{2D/v_x} \qquad (4)$$

with $\lambda_- \leq 0$ and $\lambda_+ \geq 0$. The integration constants $C_\pm$ are deduced from the boundary conditions at $x = 0$ and $x = a$. In the present experiments, $(\lambda_+ - \lambda_-)a \gg 1$ and we restrict the analysis to small values of the abscissa ($x \ll a$). Then, the second exponential in eq 3 can be neglected (see Supporting Information):

$$\tilde{F}(x, q) = \tilde{F}(0, q) \exp\left(\frac{1 - \sqrt{1 + 4D^2 q^2/v_x^2}}{2D/v_x}x\right), 0 \leq x \ll a \quad (5)$$

Noticeably, when the mass flux along x is dominated by migration (i.e., in the $2Dq/v_x \ll 1$ limit), the stationary 2D migration−diffusion pattern in eq 5 becomes[25]

$$\tilde{F}(x, q) = \tilde{F}(0, q) \exp\left(-\frac{Dq^2}{v_x}x\right) \qquad (6)$$

Experimentally, the recorded fluorescence intensity stationary pattern $I(x, y)$ is proportional to the concentration $F(x,y)$ when $\mathbf{F}$ is diluted enough. Its Fourier transform obeys

(25) After identification of x with $v_x t$, the latter equation is equivalent to the time-dependent solution for unidimensional diffusion: $\tilde{F}(t, q) = \tilde{F}(0, q) \exp(-Dq^2 t)$.

$$\frac{\tilde{I}(x, q)}{\tilde{I}(x, 0)} = \frac{\tilde{F}(0, q)}{\tilde{F}(0, 0)} \exp\left(\frac{1 - \sqrt{1 + 4D^2 q^2/v_x^2}}{2D/v_x}x\right) \qquad (7)$$

which relates the experimentally accessible normalized Fourier modes of the fluorescence intensity pattern to the normalized Fourier modes of the $\mathbf{F}$ concentration profile at $x = 0$.

Consequently, the diffusion coefficient can straightforwardly be extracted from the stationary migration−diffusion fluorescence pattern obtained in the present approach. A spatial Fourier transform along y is applied on the recorded intensity profile, and the analysis of the spatial dependence of simple exponential fits directly gives access to D provided that the analyte velocity v_x is known. In addition to the facilitated analytic extraction of the diffusion coefficients, the Fourier approach offers two other advantages: (i) It is a multiscale analysis that allows, for example, us to determine whether diffusion is length scale-dependent or not. (ii) It makes data retrieval independent of the shape of the initial concentration profiles, which only affects the amplitudes of the exponential decays. This last feature is particularly absent in the direct analysis of peak broadening, which could make diffusion coefficient measurement delicate in the case of nonregular peak shapes.

In view of the linearity of the Fourier transform, the preceding calculations are also valid for a mixture of N noninteracting species with a brightness Q_j. In particular, eq 7 yields

$$\frac{\tilde{I}(x, q)}{\tilde{I}(x, 0)} = \frac{1}{\displaystyle\sum_{j=1}^{N} Q_j \tilde{F}_j(0, 0)} \sum_{j=1}^{N} Q_j \tilde{F}_j(0, q)$$

$$\exp\left(\frac{1 - \sqrt{1 + 4D_j^2 q^2/v_{x,j}^2}}{2D/v_{x,j}}x\right) \quad (8)$$

In relation to mixture analysis, eq 8 shows that the information related to the diffusion coefficients of the mixture components is contained in the relaxation rate of the Fourier transform only. Moreover, the mixture composition can be extracted from the amplitudes of the zeroth Fourier mode ($q = 0$) associated with individual Fourier mode decays. Indeed, $\tilde{F}_j(0, 0) = 1/(2\pi)^{1/2} \int_{-\infty}^{\infty} F(0, y) \, \mathrm{d}y$ is the integrated concentration of species $\mathbf{F}_j$ over the device width at $x = 0$, which is proportional to the $\mathbf{F}_j$ concentration in the injected mixture.

EXPERIMENTAL SECTION

Reagents and Solutions. Fluorescein, Hepes, and 1 M NaOH solution were purchased from Sigma-Aldrich (St. Louis, MO) and YOYO-1 from Invitrogen (Carlsbad, CA). Single-stranded oligonucleotides−unlabeled C100, rhodamine green-labeled rhg-13, rhg-27, and rhg-105, and texas red-labeled tex-9, tex-9$_m$, and tex-9$_M$−were synthesized and HPLC purified by IBA (Göttingen, Germany). Sequences are given in Table S-2 (Supporting Information) and the figure in each molecule name indicates the strand length in bases. Double-stranded DNA fragments, 151, 438, and 1257 bp in length, were synthesized by PCR using HPLC-grade primers from IBA and λ-DNA as a template (see Supporting
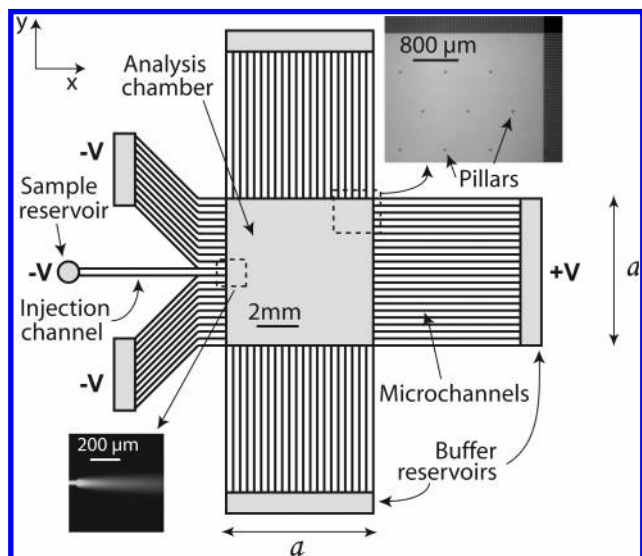
Figure 2. Top view of the PDMS microfabricated chip used for continuous electrophoresis. A uniform electric field $\vec{E} = E_x \vec{u}_x$ is generated in the analysis chamber by applying a voltage drop between the sample and buffer reservoirs on the left side ($-V$) and the buffer reservoir on the right side ($+V$). Highly resistive 20-μm-wide, 7.5-mm-long microfluidic channels spaced by 20-μm large PDMS walls ensure electric field homogeneity.[36−39] These channels also prevent electrolytically generated bubbles and uncontrolled fluid flows to disturb measurements. The 30-μm-diameter posts, arranged on an hexagonal lattice with a spacing of 800 μm, fill the analysis chamber and prevent its collapse.[37] Application of a voltage drop between the buffer reservoirs along the y axis can also be used to generate a uniform electric field along y in the analysis chamber for control time-based experiments.

Information). Agarose MP was purchased from Roche (Basel, Switzerland) and poly(dimethylacrylamide) (PDMA) of average molecular mass 3 MDa was a kind gift of J. Weber (Institut Curie, Paris, France).[26]

Solutions were prepared using water purified through a Direct-Q 5 (Millipore, Billerica, MA). Fluorescein (5 μM), fluorescent oligonucleotides (1−10 μM), and dsDNA were all dissolved in the 25/50 mM NaOH/Hepes pH 7.5 low-conductivity buffer and quantified by UV absorption spectrometry. dsDNA was subsequently stained with YOYO-1 (5 μM in YOYO-1; 1:15 dye/bp molar ratio) and incubated 30 min at room temperature. To eliminate dye-induced DNA precipitates,[27] a 10-min centrifugation at 14000 rpm was finally performed and the pellet discarded.

Chip Microfabrication. The device was composed of a circular glass coverslip (0.17 mm thick, 40-mm diameter; Menzel-Gläser, Germany) and two ∼3-mm-thick, cross-linked PDMS layers. The elastomeric bottom stamp, in contact with the glass, contained the thin analysis chamber connected to six reservoirs through arrays of microchannels (Figures 2 and S-1). On top of it, a second PDMS stamp was used to shape four macroreservoirs accommodating four electrodes and ensuring a sufficient buffer volume to keep pH constant during the experiment.

The bottom layer fabrication was decomposed in two steps (see Supporting Information for a detailed protocol). First, a positive

PDMS master with the microfluidic channels was obtained using classical soft lithography protocols.[28] The reservoirs were cut out under a stereomicroscope. Second, a negative epoxy master was fabricated by countermolding of the PDMS master. It included the reservoirs and the microfluidic channels and was used for routine production of the PDMS bottom layer, greatly reducing fabrication time. Eventually, the cured PDMS bottom layer and the coverslip were oxidized in an air plasma cleaner (PDC-002, Harrick Plasma, Ithaca, NY) for 1 min at $(2−3) \times 10^{-4}$ bar and gently brought into contact.

Device Filling, Final Assembly, and Storage. Experiments were performed in either 1% (w/w) agarose or 0.1% (w/w) PDMA, each medium being buffered with 25/50 mM NaOH/Hepes pH 7.5.

Filling the chip with an aqueous solution immediately after the preceding assembly made the central chamber ceiling collapse under capillary forces. Consequently, in order to decrease the surface hydrophilicity due to the plasma treatment, the assembled chip was cured for 45 min at 60 °C, thus allowing un-cross-linked PDMS chains to rearrange.[29] Next, the air dissolved in the PDMS was pumped for 45 min at 50 mbar at room temperature and the filling medium was added to the six reservoirs, which resulted in the autonomous and controlled loading of the device.[30] Note that, in the case of 1% agarose, the chip was thermostated at 40 °C during the filling step and subsequently cooled to 20 °C. For 0.1% PDMA, the device was first loaded with 1% PDMA at room temperature and incubated overnight. Then, just before use, the medium was changed by suction for 0.1% PDMA. Eventually, the 0.1% PDMA solution was replaced by 1% PDMA for overnight storage.

After completion of the filling operations, the PDMS top layer was cleaned with ethanol and placed over the bottom one to delimitate the four electrode compartments. The filled and assembled chips were stored, before and after use, in a water vapor-saturated atmosphere at 4 °C. The 0.1% PDMA devices presented a longer life time than the agarose ones, up to several weeks.

Instrumentation. Four platinum electrodes (0.2-mm diameter; Goodfellow, Lille, France) were placed inside the buffer reservoirs to generate orthogonal voltage drops. They were mounted on a plastic piece and connected through 1000-V-resistant cables to two electrophoresis power supplies (E835 300 V and E815 1500 V; Consort, Turnhout, Belgium). The two resulting electric fields were respectively directed along the x and y axes. They could be switched on/off and their polarity inverted by a homemade device equipped with AQV258(A) photoMOS relays (Matsushita Electric Works, Osaka, Japan) and controlled by the acquisition software. The current in each line, in the 1−300-μA range, was monitored with multimeters.

To dissipate Joule heating upon voltage application, the bottom glass surface of the chip was placed on a 0.8-mm-thick copper slide in which a hole, 2-mm diameter, had been drilled for observation with the microscope. This copper slide was mounted

(26) For an example of synthesis protocol, see: Cadix, A.; Chassenieux, C.; Lafuma, F.; Lequeux, F. *Macromolecules* **2005**, *38*, 527−536.

(27) Carlsson, C.; Jonsson, M.; Akerman, B. *Nucleic Acids Res.* **1995**, *23*, 2413−2420.

(28) Duffy, D. C.; McDonald, J. C.; Schueller, O. J. A.; Whitesides, G. M. *Anal. Chem.* **1998**, *70*, 4974−4984.

(29) Ng Lee, J.; Park, C.; Whitesides, G. M. *Anal. Chem.* **2003**, *75*, 6544−6554.

(30) Ito, T.; Inoue, A.; Sato, K.; Hosokawa, K.; Maeda, M. *Anal. Chem.* **2005**, *77*, 4759−4764.

on an aluminum block thermostated with a ± 0.2 °C precision by two thermoelectric Peltier coolers (CP 1.0-63-05L-RTV; Melcor, Trenton, NJ). The temperature was monitored using a TCS610 thermistor (Wavelength Electronics, Bozeman, MT) and the feedback loop was driven by a MPT10000 temperature controller (Wavelength Electronics), which received settings from the computer through a usb-1208FS I/O board (Measurement Computing, Norton, MA). Under our experimental conditions, at 20 °C, Joule heating was efficiently dissipated for electric currents below 300 μA (see Figure S-6), this latter value corresponding to an electric field of 2.66×10^4 V m^{-1} inside the analysis chamber (1000 V between the electrodes).

Epifluorescence imaging of the chip was achieved at 24 Hz on a homemade microscope equipped with a 100-W Xe lamp (LOT-Oriel, Palaiseau, France), a wide-band hot mirror (Thorlabs, Newton, NJ), a set of filters (excitation HQ 495/30, dichroic 520 DCXR, emission HQ 560/80M; Chroma Technology, Rockingham, VT), a 10× objective (Fluar NA 0.5; Zeiss, Le Pecq, France), and a CCD camera (CV-M4+CL 2/3 in.; JAI, Copenhagen, Denmark). The field of view was ~1 mm. To check the linearity of the video signal, the microdevice was filled with increasing fluorescein concentrations and illuminated at low intensities, thus avoiding photobleaching. For the whole dynamic range of the camera, the response was linear between 0.5 and 20 μM. The quantum yield of fluorescence being constant in this dilution range, the signal in each pixel was therefore assumed to be directly proportional to the solute concentration.

Interfacing of the electric field and temperature controllers, as well as video acquisition, were performed by a homemade program written in C.

Measurement of Diffusion Coefficient. All the loading analyte solutions contained 10% (v/v) glycerol to prevent dilution in the buffer reservoir of the top PDMS layer. Typically, 1-μL volumes were loaded into the sample reservoir (Figure 2), allowing for 15 min to 1 h of continuous injection (depending on the applied voltage). Additionally, 0.1% (w/w) PDMA was added to the sample when experiments were carried out in the presence of this polymer.

A stationary migration−diffusion pattern was generated by applying a permanent voltage drop between the two reservoirs located along the x axis, values between 10 and 1000 V resulting in electric fields between 266 and 2.66×10^4 V m^{-1} in the analysis chamber. A source image was then recorded by averaging over typically 240 frames (total integration time of 10 s). The chip autofluorescence was subsequently substracted to these data, and noise reduction was obtained by performing a sliding average along the x axis (usually over 10-pixel lines). Final corrected $I(x, y)$ images were 1024 or 512 pixels wide in y, which corresponded to on-chip distances l_y of 875.50 or 437.75 μm, respectively (Figure 3).

Discrete fast Fourier transform using periodic boundary conditions was next performed along y to yield a Fourier-transformed image $\tilde{I}(x, n)$. Note that the n index accounts here for the $q_n = 2\pi n/l_y$ discrete spatial frequency. Then, each Fourier mode was normalized by the zeroth Fourier mode $\tilde{I}(x, 0)$ to correct from illumination inhomogeneities (see Supporting Information), and data in the region of inhomogeneous electric field, up to $l_0 = 40$ μm after the chamber entry, were discarded (vide infra; See also Figure S-8).
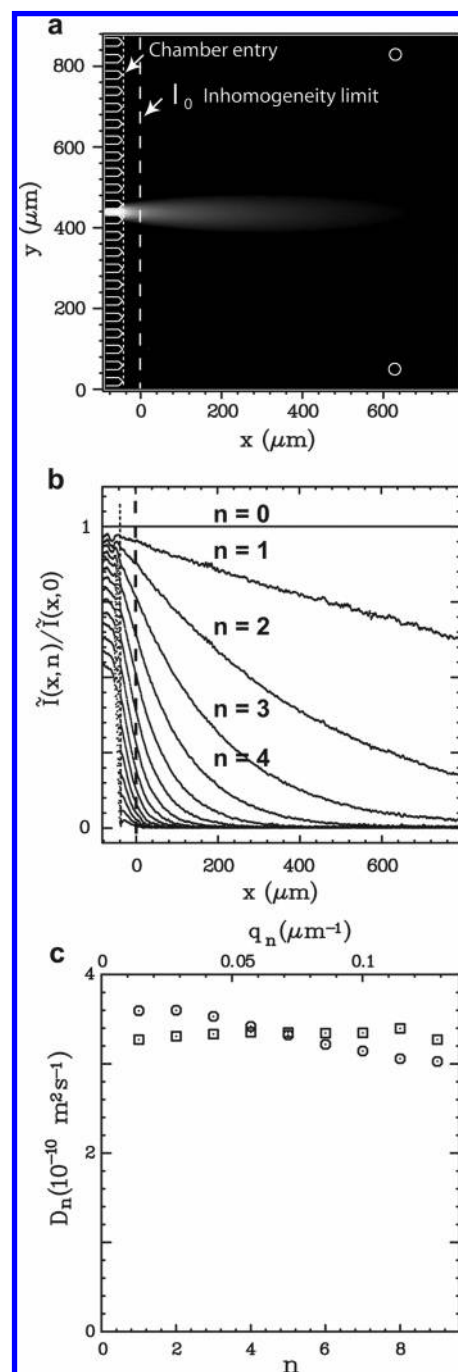
Figure 3. Successive steps of the 1D Fourier transform analysis used to extract the diffusion coefficient of a fluorescent analyte from a continuous experiment. (a) Stationary migration−diffusion pattern for 5 μM fluorescein when an electric field of 8×10^3 V m^{-1} (v_x = 145 μm s^{-1}) is applied left to right in NaOH/Hepes 25/50 mM, pH 7.5, 0.1% (w/w) PDMA buffer at 20 °C. The microfabricated channels and pillar profiles are highlighted with solid lines. The vertical dotted line corresponds to the boundary between the resistive channels and the analysis chamber. The dashed line emphasizes the upstream limit for homogeneous electric field. (b) Spatial dependence along x of the $\tilde{I}(x, n)/\tilde{I}(x, 0)$ normalized Fourier modes resulting from Fourier transform along y of the preceding image. (c) Experimental (○) and simulated (□; see Supporting Information) diffusion coefficients as a function of the Fourier index n (bottom scale) or of the spatial frequency q_n (upper scale). Data are obtained by monoexponential fitting of the above normalized Fourier mode, discarding all the points with a negative abscissa (i.e., left to the dashed line).

Each normalized Fourier mode was subsequently fitted with a two-parameter exponential function $\tilde{I}(x,n)/\tilde{I}(x,0) = a_n e^{-l_n x}$. For each fit, residuals were calculated and the signal-to-noise ratio (S/N) was quantified as a_n divided by the maximal residual amplitude. Only data satisfying S/N > 2 were retained for further analysis. Using eq 5, the diffusion coefficient D_n associated with the Fourier mode n was extracted from the exponential decay rate l_n as $D_n = l_n v_x/(l_n^2 - q_n^2)$, where v_x is here the analyte velocity along x, measured after each experiment by recording the injection of a front of solute into the analysis chamber. More precisely, any fluorescent molecule was first washed away by transiently applying an electric field along y. Then, $\vec{E} = E_x \vec{u}_x$ was switched on and the displacement of the fluorescent profile along x was recorded. Finally, the front position was plotted versus time to yield v_x.[31]

Data treatment was completed by computing the average diffusion coefficient $\langle D \rangle = (\sum_{n=1}^N a_n l_n D_n)/(\sum_{n=1}^N a_n l_n)$, where N is the number of fitted Fourier modes. The weighting reflects here that the confidence of an exponential fit is proportional to its curvature l_n and to its amplitude a_n. The corresponding standard deviation was hence evaluated as $\sigma_{\langle D \rangle}^2 = (\sum_{n=1}^N a_n l_n D_n^2)/(\sum_{n=1}^N a_n l_n) - \langle D \rangle^2$.

Binary Mixture Analysis. The normalized Fourier modes of the fluorescence pattern were fitted with a biexponential function $\tilde{I}(x,n)/\tilde{I}(x,0) = a_{1,n} e^{-l_{1,n} x} + a_{2,n} e^{-l_{2,n} x}$ to extract the individual diffusion coefficients $D_{j,n}$ as well as the relative proportion of the two components of the binary mixture.

The diffusion coefficients $D_{j,n}$ were calculated from the spatial decays as for the single component (vide supra) and the measured average mixture velocity v_x.[32] The relative proportions of the two species were measured by the ratio $\alpha_{exp} = \tilde{F}_1(0,0)/\tilde{F}_2(0,0)$. A first possibility to access the $\tilde{F}_j(0,0)$ terms should be to determine the $a_{j,0}$. However, biexponential fitting was not reliable for $n \leq 2$.[33] Thus, direct access to the $a_{j,0}$ was not possible and an alternative road was explored. We observed that the concentration profiles $F_j(0,y)$ were Gaussian (Figure S-8e).[34] Then, we deduced their Fourier transform $\tilde{F}_j(0,n)$ to also be Gaussian. We consequently fit the dependence of the amplitudes $a_{j,n}$ on the mode index n with Gaussian functions $\gamma_j e^{-\nu_j n^2}$ and rely on their intersection with the ordinates axis to extract $a_{1,0}$ and $a_{2,0}$. Eventually, the ratio of the concentrations in $\mathbf{F}_1$ and $\mathbf{F}_2$ in the injected sample was computed as $\alpha_{exp} = (Q_2/Q_1)(a_{1,0}/a_{2,0})$.

FCS Experiments. FCS experiments were performed on a home-built, two-photon epi-illumination setup (dichroic filter 680DCSPXR; Chroma Technology).[35] A 50 nM fluorescent solution was excited at 780 nm with a Ti:sapphire laser (Mira 900; Coherent, Auburn, CA) using a $60\times$ objective (UPlan apo, NA 1.2; Olympus, Rungis, France). The fluorescence light, collected with the same objective and passed through an emission filter (560/80M; Chroma Technology), was then split to allow simultaneous acquisition on two avalanche photodiodes (SPCM-AQR-14 APD; Perkin-Elmer, Wellesley, MA). For each run, the cross-correlation function from the two APD signals was calculated by an ALV-6000 digital correlator (ALV, Langen, Germany). Thirty runs of 30 s were averaged to yield the final data. This last cross-correlation function was subsequently fitted with $G(t) = 1/[\bar{N}(1 + t/\tau_D)]$, where $\bar{N}$, the average number of molecules in the excitation volume and $\tau_D = \omega_0^2/(8D)$, the solute diffusion time, were the two floating parameters. The diffusion coefficient D was finally extracted from τ_D using the calibrated laser beam-waist at the focal point ω_0 (here 430 nm).

Extraction of the Association Constant K between Complementary Oligonucleotides. Fluorescence measurements were performed on a LPS 220 spectrofluorometer (Photon Technology International, Birmingham, NJ) using a quartz cuvette with a 1-cm optical path. Excitation and emission wavelengths were set at 587 and 612 nm, respectively, with a bandwidth of 4 nm. After each experiment, the cuvette was cleaned for 15 min in a 1% (v/v) solution of Hellmanex soap (Hellma, Mülheim, Germany) in an ultrasonic bath.

The 400 μL of 50 nM texas red-labeled oligonucleotide was equilibrated at 10 °C in 25/50 mM NaOH/Hepes, pH 7.5, buffer supplemented with 10 μg/mL sonicated DNA salmon sperm (Fluka), to prevent oligonucleotide adsorption, and 0.1% (w/w) PDMA. The decrease in fluorescence intensity, associated with the hybridization process, was recorded while increasing concentrations of C100 were added at constant texas red-labeled oligonucleotide concentration. Data were then analyzed from

$$\frac{I}{I_0} = 1 - \frac{1}{2}(1 - \mathcal{Q})\left\{ \left(1 + \xi + \frac{1}{KR_0}\right) - \sqrt{\left(1 + \xi + \frac{1}{KR_0}\right)^2 - 4\xi} \right\} \quad (9)$$

where I is the fluorescence intensity at equilibrium when ξ equivalents of C100 have been added to the solution, $\mathcal{Q}$ is the relative brightness of the complex with regard to the free 9-mer probe one, I_0 is the intensity at the beginning of the experiment, and R_0 is the initial concentration in texas red-labeled oligonucleotide. R_0 being known, we extracted K and $\mathcal{Q}$ by a least-squares fit of our data with eq 9.

Safety Considerations. YOYO-1 is a possible mutagen; caution should be held when manipulating it. High-voltages may cause electric shock; high-voltage-resistant cables and grounded material must be used.

RESULTS AND DISCUSSION

Velocity Homogeneity inside the Analysis Chamber. To benefit from the simple data treatment relying on eq 7, the velocity

(31) The front position was calculated by correlating each intensity profile with its symetric. See, for example: Gosse, C.; Croquette, V. *Biophys. J.* **2002**, *82*, 3314−3329.

(32) The electrophoretic mobilities of the dsDNA samples were identical, as expected for free-draining polyelectrolytes migrating in free solution.[50,52] Similarly, concerning the 9-mer probe used in the hybridization assay, we could not observe any modification of migration velocity upon binding to its long ssDNA target. For other analytes, such as proteins, one would need to measure both individual $v_{x,j}$ prior to $D_{j,n}$ extraction.

(33) The whole pool of normalized Fourier modes was appropriate for mixture analysis. All the normalized Fourier modes are fitted in parallel with a monoexponential and a biexponential function. All the modes giving satisfactory residuals with the simpler fit were discarded, the parameters extracted from their biexponential analysis being considered unreliable (Figure S-9).

(34) The Gaussian shape reflects the channel one broadened by molecular diffusion and migration due to out-of-axis electric fields between the injection nozzle and the zone of homogeneous velocity (see Supporting Information).

(35) Gosse, C.; Boutorine, A.; Aujard, I.; Chami, M.; Kononov, A.; Cogné-Laage, E.; Allemand, J.-F.; Li, J.; Jullien, L. *J. Phys. Chem. B* **2004**, *108*, 6485−6497.

of the **F** solute inside the analysis chamber must be uniform and directed along x. This assumption is fulfilled when (i) the electric field itself is uniform and directed along x and (ii) the electrophoretic and electroosmotic mobilities of **F** are constant within the chamber medium.

To generate a uniform electric field along x in the analysis chamber of the present microdevice, we relied on the prism design introduced by Huang et al. (Figure 2).[36-38] In this kind of design, electric field inhomogeneities extend up to a distance l_0 far from the resistive channels ends, which typically corresponds to the lateral periodicity of the microfluidic array.[40] As a consequence, l_0 was used to define the x origin and all the points with negative abscissa were discarded before data treatment.[41]

Electrophoretic mobility is constant as soon as the filling medium is homogeneous. In contrast, the obtention of a constant electroosmotic mobility usually relies on efficient surface treatments.[42,43] In particular, our device is made of glass and PDMS and the lower and upper walls have consequently different physicochemical properties: without surface treatment, buffer flow at each interface will be different, leading to Taylor dispersion of the solute.[44-46] To circumvent these problems, two strategies have been implemented. Either we suppressed any hydrodynamic flow by working in a gel (experiments in 1% (w/w) agarose) or we reduced and smoothed electroosmosis by adding a neutral wall-adsorbing polymer to the filling aqueous solution (experiments in 0.1% (w/w) PDMA).[47] Under both experimental conditions, we

(36) Huang, L. R.; Tegenfeldt, J. O.; Kraeft, J. J.; Sturm, J. C.; Austin, R. H.; Cox, E. C. *Nat. Biotechnol.* **2002**, *20*, 1048−1051.

(37) Zhang, C.-X.; Manz, A. *Anal. Chem.* **2003**, *75*, 5759−5766.

(38) Huang, L. R.; Tegenfeldt, J. O.; Kraeft, J. J.; Sturm, J. C.; Austin, R. H.; Cox, E. C. *Tech. Dig.-Int. Electron Devices Meet.* **2001**, 363−366.

(39) The bowed channels located on the injection side of the device were shortened to compensate for width reduction, thus keeping their overall resistance constant.

(40) Electric potential profiles were calculated by finite element method simulations and found in good agreement with this estimate. The electric field is constant and directed along the x-axis everywhere beyond a $l_0 = 40\ \mu m$ limit inside the chamber boundaries (Figure S-7). We checked on chip these predictions by recording the migration of long and thin bands of YOYO-1-stained 1257-bp dsDNA. When prepared along y and eluted in the x direction, a stripe of this weakly diffusing fluorophore moves straight and stays normal to $\bar{u}_x$, thus confirming the field homogeneity and direction.

(41) The pillars that sustain the PDMS chamber ceiling also induce a perturbation of the electric potential. However, it is of the order of their diameter (i.e., 30 μm) and exerts no significant influence on the analyte migration.

(42) Hjertén, S. *J. Chromatogr., A* **1985**, *347*, 191−198.

(43) Doherty, E. A. S.; Berglund, K. D.; Buchholz, B. A.; Kourkine, I. V.; Przybycien; T. M.; Tilton, R. D.; Barron, A. E. *Electrophoresis* **2002**, *23*, 2766−2776.

(44) Andreev, V. P.; Dubrovsky, S. G.; Stepanov, Y. V. *J. Microcolumn Sep.* **1997**, *9*, 443−450.

(45) Ross, D.; Johnson, T.J.; Locascio, L.E. *Anal. Chem.* **2001**, *73*, 2509−2515.

(46) Bianchi, F.; Wagner, F.; Hoffmann, P.; Girault, H. H. *Anal. Chem.* **2001**, *73*, 829−836.

(47) By comparing the fluorescein electrophoretic velocity in the two media, the remaining electroosmotic mobility μ_{EO} in 0.1 % PDMA was evaluated to be less than 10% of the apparent electrophoretic mobility for all the considered analytes; see ref 43 and: Zhang, P.; Ren, J. *Anal. Chim. Acta* **2004**, *507*, 179−184.

(48) To quantify the electroosmotic dispersive contribution that could superimpose to Brownian diffusion, we designed a series of control time-based experiments where the apparent diffusion coefficients are extracted from the time evolution along the y-axis of an x-invariant concentration profile. Measurements were performed either in the absence or in the presence of a transverse alternative electric field E_y (see Supporting Information).[7,45] For the two filling media, the good agreement between the apparent diffusion coefficients extracted from time-based as well as continuous experiments strongly supports the absence of any significant electric field-induced dispersion in the present systems.

did not observe any significant electric field-induced dispersion:[48] The electrophoretic and electroosmotic mobilities were constant in the three dimensions.

Diffusion Coefficient Measurement. Figure 3 displays a typical continuous experiment and the subsequent data treatment to extract the diffusion coefficient of an analyte. A permanent voltage drop of 300 V is applied between the electrodes, which corresponds to $E_x = 8 \times 10^3$ V m^{-1} inside the analysis chamber filled with NaOH/Hepes 25/50 mM, pH 7.5, 0.1% (w/w) PDMA buffer. A stationary migration−diffusion fluorescence pattern establishes after a time delay in the order of l_x/v_x, where $l_x \sim$ 800 μm is the image length along x. Here, the solute velocity $v_x =$ 145 μm·s^{-1} results in a 5.5-s transient. The profile $I(x, y)$ of fluorescence intensity is next recorded (Figure 3a) and Fourier-transformed along the y axis to obtain the x spatial dependence of each discrete Fourier mode $\tilde{I}(x, n)$ (see also Figure S-8). To correct from illumination inhomogeneities as well as from **F** photobleaching during elution, we subsequently divide each $\tilde{I}(x, n)$ by $\tilde{I}(x, 0)$ (see Figure 3b and Supporting Information). Then, the normalized Fourier modes $\tilde{I}(x, n)/\tilde{I}(x, 0)$ are fitted with monoexponential functions, yielding satisfactory residuals for all the investigated orders (Figure S-8). Once the velocity of **F** along x has been measured (see Experimental Section), each relaxation rate extracted from the exponential fit is used to calculate the diffusion coefficient D_n associated with the Fourier mode n. Eventually, the average diffusion coefficient $\langle D \rangle$ is computed by averaging over n (see Experimental Section). After validation of the latter procedure for data processing (see Supporting Information), we compared the values of diffusion coefficients obtained with the present approach with the literature results as well as with our own measurements derived from other types of experiments.

We first evaluated the interest of the present approach to characterize a diffusive behavior. Figure 3c displays the dependence of the diffusion coefficients D_n on the Fourier mode n for fluorescein in the buffer supplemented with 0.1% (w/w) PDMA. Despite a 10% dispersion of the data, that might result from incomplete illumination correction or slight velocity inhomogeneities, the D_n diffusion coefficients are constant over nine Fourier modes, corresponding to a 15−140 μm spatial range. This result is in line with the anticipated purely diffusive process at all the length scales for this fluorophore in a free solution.[49] In addition, the extracted average value of the diffusion coefficient $\langle D \rangle =$ $(340 \pm 30) \times 10^{-12}$ m ^{2} s^{-1} fairly agrees with literature results.[7]

Second, we measured D for analytes with molecular masses between 330 and 8×10^5 Da to investigate the operating range and the measurement accuracy of the device. Table 1 compares, for fluorescein and three rhodamine green-labeled single-stranded oligonucleotides, the average diffusion coefficients obtained with the present continuous method to the ones from on chip zero-field time-based experiments (see Supporting Information) or FCS measurements. A 1% agarose gel was here used to totally suppress electroosmosis. The three techniques provide coherent results within experimental error, hence, validating the continuous measurement of diffusion coefficients in the absence of any

(49) As evaluated from Mark−Houwink parameters (Heller, C. *Electrophoresis* **1999**, *20*, 1962−1977), 0.1 % (w/w) PDMA approximately corresponds to the entanglement threshold for the 3-MDa polymer. Thus, slight viscosity or steric effects might be present.

Table 1. Averaged Diffusion Coefficients ⟨D⟩ (10⁻¹² m² s⁻¹) of Fluorescein and Rhodamine Green-Labeled Oligonucleotides in NaOH/Hepes 25/50 mM, pH 7.5, 1% (w/w) Agarose Medium at 20 °C[a]

	fluorescein	rhg-13	rhg-27	rhg-105
continuous[b]	310 ± 24	100 ± 10	77 ± 5	39 ± 4
time-based	320 ± 20	107 ± 6	75 ± 4	40 ± 2
FCS	350 ± 70	140 ± 0	86 ± 8	44 ± 5

[a] Measurements were performed on chip and by FCS. In the former case, values were extracted by Fourier transform analysis of continuous and zero-field time-based (see Supporting Information) experiments. Errors correspond to standard deviation. [b] Averaged from different experiments with v_x ranging from 10 to 150 μm s⁻¹.

Table 2. Averaged Diffusion Coefficients ⟨D⟩ (10⁻¹² m² s⁻¹) of Fluorescein, rhg-13, a 13-Bases-Long Rhodamine Green-Labeled Oligonucleotide, and YOYO-1-Stained dsDNA of Different Lengths (1:15 Dye/bp Ratio) in NaOH/Hepes 25/50 mM pH 7.5, 0.1% (w/w) PDMA Buffer at 20 °C[a]

	fluorescein	rhg-13	151 bp	438 bp	1257 bp
continuous	340 ± 30	110 ± 10	16 ± 2	9.1 ± 0.4	3.8 ± 0.7
time-based	330 ± 10	106 ± 5	17 ± 2	8.6 ± 0.8	4.2 ± 0.3
literature	380 ± 1[b]	180 ± 20[c]	26 ± 3[c]	13 ± 1[c]	6.4 ± 0.6[c]

[a] Values from Fourier transform analysis of continuous and zero-field time-based (see Supporting Information) experiments are compared with literature ones. Errors correspond to standard deviation. [b] From Culbertson et al.,[7] corrected at 20 °C. [c] Data calculated using the $D_{ssDNA} = 7.38 \times 10^{-6} N^{-0.539}$ and $D_{dsDNA} = 7.73 \times 10^{-6} N^{-0.672}$ scaling laws given by Stellwagen et al. for nonlabeled single-stranded and double-stranded DNA, N bases long.[50]

hydrodynamic flow. We next performed a series of experiments in the buffer supplemented with 0.1% (w/w) PDMA (Table 2). As shown above, we obtained a satisfactory result for fluorescein with a diffusion coefficient only 10% lower than the one determined by Culbertson et al.[7] In the case of rhg-13, ⟨D⟩ was 40% lower than the value computed from a scaling law proposed by Stellwagen and co-workers.[50] The observed discrepancy probably originates from fluorophore-labeling effects[51] and sequence-dependent contributions. Table 2 also displays diffusion coefficients measured for three YOYO-1-stained dsDNA in the 150−1500-bp range. The diffusion of duplex DNA has already been extensively studied.[50,52,53] All the existing values agree with the $D_{dsDNA} \sim AN^{-0.672}$ scaling law, where A is a constant and N the fragment length in bp.[50] Likewise, our data could be fitted by $\langle D \rangle_{dsDNA} \sim A'N^{-0.678}$ ($r^2 = 0.984$). The correct exponent obtained for this power law indicates that the 0.1% (w/w) PDMA solution has poor sieving properties and essentially behaves as a free solution. However, we here obtained $A' \sim 2/3A$. This difference is probably associated with a YOYO-1-induced increase in the DNA persistence length,
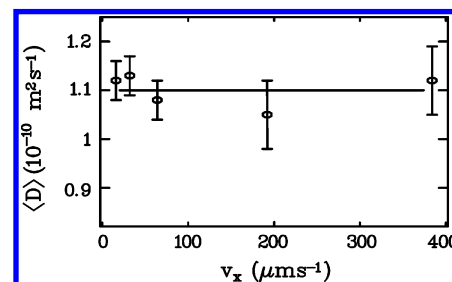
Figure 4. Dependence of the average rhg-13 diffusion coefficient on the analyte velocity v_x in NaOH/Hepes 25/50 mM, pH 7.5, 0.1% (w/w) PDMA buffer at 20 °C. The horizontal line corresponds to the value obtained by averaging the results from the 5 different experiments.

as already reported for TOTO-1-stained dsDNA at 1:5 dye/bp ratio.[54]

For a fixed field of view, a wide range of diffusion coefficients can be explored by tuning v_x. The applied electric field is therefore a valuable experimental parameter, provided that ⟨D⟩ does not depend on it. To address the latter issue, we performed a series of continuous experiments by applying electric fields between 6.7×10^2 and 1.6×10^4 V m⁻¹, resulting in velocities in the 13.5−324 μm s⁻¹ range for rhg-13 in NaOH/Hepes 25/50 mM, pH 7.5, 0.1% (w/w) PDMA buffer at 20 °C. Within experimental error, no significant difference was observed for the measured diffusion coefficients (Figure 4).

Finally, with respect to potential high-throughput applications, one may here want to evaluate the time necessary to perform a single measurement. With the present instrumental setup, the video images are acquired during 10 s for all the considered analytes but the durations of the whole experiment range from 13 to 40 s. Indeed, the migration−diffusion pattern does not establish instantaneously and a delay is required between the beginning of the injection and the image capture: Waiting times vary according to molecular diffusion coefficients and electrophoretic mobilities, from 3 s for fluorescein to 30 s for 8×10^5 Da dsDNA. Due to similar physics and device sizes, this analysis rate is in the same order of magnitude as one of the T-sensors. Note that a significant improvement could be obtained by reducing the width of the injection channel and the field of view of the camera.

Analysis of Binary Mixtures. From an analytical point of view, differentiating a mixture from a pure sample is a valuable issue. For instance, in some ligand−receptor titration experiments, each compound relative abundance is quantified using a diffusion coefficient-based identification.[2−4] Similar questions have also been addressed in FRAP experiments where labeled proteins are often involved in molecular assemblies of various sizes.[10] In these last cases, data were directly extracted from the recorded image, which required complex fitting algorithms.[55,56] Once again, 1D Fourier transform analysis is more straightforward: A binary mixture can be characterized with a simple and robust biexponential fit.

To evaluate the present approach for analyzing binary mixtures, we first performed a series of continuous experiments with a

(50) Stellwagen, E.; Lu, Y.; Stellwagen, N. C. *Biochemistry* **2003**, *42*, 11745−11750.

(51) Pappaert, K.; Biesemans, J.; Clicq, D.; Vankrunkelsven, S.; Desmet, G. *Lab Chip* **2005**, *5*, 1104−1110.
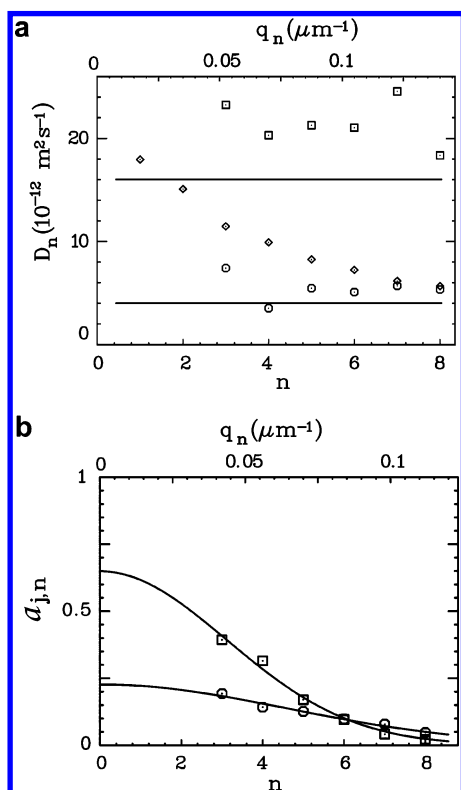
(52) Nkodo, A. E.; Garnier, J. M.; Tinland, B.; Ren, H.; Desruisseaux, C.; McCormick, L. C.; Drouin, G.; Slater, G. W. *Electrophoresis* **2001**, *22*, 2424−2432.

(53) Liu, M. K.; Giddings, J. C. *Macromolecules* **1993**, *26*, 3576−3588.

(54) Smith, D. E.; Perkins, T. T.; Chu, S. *Macromolecules* **1996**, *29*, 1372−1373.

(55) Gordon, G. W.; Chazotte, B.; Wang, X. F.; Herman, B. *Biophys. J.* **1995**, *68*, 766−778.

(56) Periasamy, N.; Verkman, A. S. *Biophys. J.* **1998**, *75*, 557−567.

Figure 5. Analysis of a binary mixture composed of 151 and 1257 bp YOYO-1-stained dsDNA (1:15 dye/bp ratio) in relative abundance $\alpha = 2.2$. The corresponding stationary migration−diffusion pattern was obtained by applying an electric field $E_x = 266$ V m^{-1} ($v_x = 4.8$ μm s^{-1}) in an analysis chamber filled with NaOH/Hepes 25/50 mM, 0.1% (w/w) PDMA buffer at 20 °C. (a) Diffusion coefficients as a function of the Fourier index n or of the spatial frequency q_n. Data were extracted by either monoexponential ($\diamond$; see also Supporting Information) or biexponential fits ($\square$ for 151 bp, $\bigcirc$ for 1257 bp) of the normalized Fourier modes. The horizontal lines correspond to the diffusion coefficients measured on pure samples (Table 2). In the case of the monoexponential fit, note that the inaccuracy is evidenced by observing that the extracted apparent diffusion coefficient decreased with n: Close to the value expected for the fastest diffusive species for the lowest n values, it tends to the one associated with the slowest diffusive analyte at large enough n values. (b) Corresponding dependence of the preexponential amplitudes resulting from the above biexponential fit. Solid lines correspond to Gaussian fits (see Experimental Section).

mixture of two YOYO-1-stained dsDNA fragments, 151 and 1257 bp long, in 0.1% (w/w) PDMA buffer. Their diffusion coefficients differed by a factor 4 (Table 2), which made discrimination possible.[57] The normalized 1D Fourier modes $\tilde{I}(x, n)/\tilde{I}(x, 0)$ extracted from the corresponding stationary migration−diffusion pattern were fitted with a biexponential function.[58] For a given Fourier mode, two relaxation rates were extracted and the corresponding diffusion coefficients $D_{1,n}$ and $D_{2,n}$ were computed. For unambiguously non-monoexponential relaxations, the extracted values were in satisfactory agreement with the diffusion coefficients measured from pure 151- and 1257-bp-long dsDNA samples (Figure 5a, Tables 2 and 3). Additionally, we also analyzed the binary mixture using the amplitudes of the two exponential contributions. In the present analysis, the relative abundance of two species with concentrations F_1 and F_2, $\alpha = F_1/F_2$, can be computed from the respective brightnesses Q_j and the zeroth Fourier mode preexponential amplitudes $a_{j,0}$: $\alpha = Q_2/Q_1$

Table 3. Analysis of Two Binary Mixtures of YOYO-1-Stained 151- and 1257-bp DsDNA in NaOH/Hepes 25/50 mM, pH 7.5, 0.1% (w/w) PDMA Buffer at 20 °C[a]

α	α_{exp}	$\langle D \rangle_{151\text{bp}}$	$\langle D \rangle_{1257\text{bp}}$
2.2	3 ± 1	21 ± 3	5 ± 1
0.7	0.5 ± 0.2	16 ± 6	4 ± 1

[a] α accounts for the actual relative abundance of the two fragments (151 bp/1257 bp). The experimental relative abundance α_{exp} and the average diffusion coefficients $\langle D \rangle_j$ (10^{-12} m^2 s^{-1}) are extracted from biexponential fits of the normalized Fourier modes. Errors correspond to standard deviation.

$\times$ $a_{1,0}/a_{2,0}$ (see Experimental Section). Considering that YOYO-1 has a similar affinity per base pair for 151- and 1257-bp-long dsDNA fragments and that its brightness does not depend on the dsDNA length, we could set $Q_2/Q_1 = 1$ when concentrations were defined in bp mol/L. Table 3 displays the results obtained from analyzing the composition of two different mixtures. For both, the extracted α_{exp} values correspond to the expected relative abundance α within 30%.

We also applied the diffusion-based analysis of binary mixtures to screen the affinity of a compound library for a given target molecule. More precisely, we studied the extent of hybridization between three texas red-labeled 9-mer oligonucleotides and C100, a 100-mer ssDNA.[59] The first probe, tex-9, was perfectly complementary to C100, whereas a mismatched base pair in tex-9$_m$ and tex-9$_M$ was expected to, respectively, slightly (m) and heavily (M) impede duplex formation (see Table S-2 for sequences).[60] Titrations by fluorescence spectroscopy confirmed the expected trend: We found $K_{\text{tex}-9} = (3 \pm 1) \times 10^5$, $K_{\text{tex}-9_m} = (3 \pm 1) \times 10^5$, and $K_{\text{tex}-9_M} < 10^4$ for the association constants between C100 and the interrogated oligonucleotides. Next, each equilibrated mixture, containing 1 μM labeled 9-mer and 5 μM C100 in NaOH/Hepes 25/50 mM, 0.1% (w/w) PDMA buffer, was sequentially analyzed on chip at 10 °C. The resulting stationary migration−diffusion images were recorded, Fourier-transformed along *y*, and the

(57) In the present approach, the differentiation between two species $\mathbf{F}_j$ relies on their respective $D_j/v_{x,j}$ ratio. Using the Einstein equation $D_j = kT/\xi_j$ and of the velocity $\vec{v}_j = v_{x,j}\vec{u}_x = (\mu_j + \mu_{\text{EO}})E_x\vec{u}_x$, this discriminating factor develops as $D_j/v_{x,j} = kT/[(z_j + \mu_{\text{EO}} \xi_j)E_x]$, where ξ_j and z_j are the respective $\mathbf{F}_j$ solute molecular friction coefficient and charge. In principle, it should consequently always be possible to discriminate the two components in a binary mixture. Indeed, even when dealing with uncharged species, one can tune the surface properties of the microdevice to generate an appropriate electroosmotic flow (see, for instance: Liu, Y.; Fanguy, J. C.; Bledsoe, J. M.; Henry, C. S. *Anal. Chem.* **2000**, *72*, 5939−5944). Polyelectrolytes such as DNA behave like free-draining coils when submitted to an electric field in free solution. The preceding Nernst−Einstein relation does not apply anymore[52] and must be replaced by $\{D_j/v_{x,j}\}_{\text{free}-\text{draining}} = \{kT/[(z_K + \mu_{\text{EO}}\xi_K)\xi_K)E_x]\}\xi_K \mathcal{A} N_j^{-\nu}$, where ξ_K and z_K are the respective Kuhn segment molecular friction coefficient and charge and $\mathcal{A} \cdot N_j^{-\nu}$ is a Zimm-type power law for D_j.

(58) A sum of two Gaussian functions failed to fit the stationary migration−diffusion pattern in the direct space, thus emphasizing the strength of Fourier data analysis.

(59) From independent bulk measurements, we estimated the chemical relaxation time for all the injected duplexes to be at least 1 order of magnitude longer than the analysis duration. Consequently, the present technique provides information on the composition of the reactive mixture, which can be considered as frozen at equilibrium.

(60) Aboul-ela, F.; Koh, D.; Tinoco, I., Jr.; Martin, F. H. *Nucleic Acids Res.* **1985**, *13*, 4811−4825.

Table 4. Affinity Screening of Three Texas Red-Labeled 9-mer Oligonucleotides That Hybridize to a Long Target ssDNA, C100, in NaOH/Hepes 25/50 mM, pH 7.5, 0.1% (w/w) PDMA Buffer at 10 °C[a]

mixture	α_{exp}	α	$\langle D \rangle_{free\ probe}$	$\langle D \rangle_{duplex}$
tex-9	0	0	106 ± 3	
tex-9+C100	1.05 ± 0.05	1.3 ± 0.4	106 ± 3	33 ± 3
tex-9$_m$ +C100	0.83 ± 0.05	1.3 ± 0.4	106 ± 2	33 ± 3
tex-9$_M$ +C100	0.07 ± 0.05	0.05 ± 0.02	117 ± 5	0 ± 5

[a] α accounts for the relative abundance between the probe−target duplex and the free probe (duplex/free probe) as measured independently by fluorescence spectroscopy titration. The experimental relative abundance α_{exp} and the average diffusion coefficients $\langle D \rangle_j$ (10^{-12} m^2 s^{-1}) are extracted from biexponential fits of the normalized Fourier modes. Errors correspond to standard deviation.

corresponding Fourier modes were fitted with the biexponential function for a binary mixture (see Experimental Section and Figure S-10). Table 4 shows the derived relative abundance of duplex to free probe, α_{exp}, as well as the two extracted diffusion coefficients. For comparison, Table 4 also contains the relative abundance α calculated from the association constants. The agreement between the values of α_{exp} and α is again satisfactory.

The latter results particularly emphasize the efficiency of our approach for library screening or assays to detect mutations. Accurate thermodynamic information on probe−target or ligand−receptor interactions can be obtained within a few tens of seconds, provided, as it is often the case in a biological context, a large enough size difference between the two partners, but independently on brightness issues since the discriminating factor is the ratio of the diffusion coefficient to the velocity only. Additionally, the analysis is here performed in free solution and without separation, two important advantages over chromatographic or array-based techniques that usually rely on complex grafting and elution procedures.

CONCLUSION

In this paper, we introduced a continuous method for measuring on chip the diffusion coefficient of fluorescent solutes. The analytes are punctually introduced into a PDMS/glass thin chamber where they migrate along a constant and homogeneous velocity field generated by electrokinetic effects. The solute diffusion mainly manifests itself in the direction normal to elution, and the resulting stationary migration−diffusion pattern is recorded by videomicroscopy. A subsequent image analysis in the Fourier space facilitates data processing by easily providing the diffusion coefficient whatever the initial concentration profile at the injection nozzle. Moreover, this powerful multiscale analysis

can give valuable informations on length-scale-dependent behaviors or molecular weight distributions.

We have first validated our method by measuring diffusion coefficients ranging from 3×10^{-10} to 4×10^{-12} m^2 s^{-1}, which corresponds to fluorescent species with molecular masses spanning between 330 and 8×10^5 Da. We subsequently applied the present approach to straightforwardly discriminate a pure sample from a complex one. In particular, we showed that the components of a binary mixture could be identified and quantified by observing their diffusive behavior. This observation bears much significance in a pharmaceutical perspective where, during library screening, one aims at measuring, without separation if possible, the relative proportion in two states of a ligand: free or bound to a given receptor.

SUPPORTING INFORMATION AVAILABLE

Listing including the theoretical derivation of the Fourier transform of the concentration $F(x,y)$ with respect to y, the PCR protocol, a detailed microfabrication protocol, finite element method simulations, a description of time-based experiments, a detailed analysis to correct for illumination inhomogeneities, and the validation of the procedure for data processing. Supplementary tables provide the sequences of the rhodamine green-labeled oligonucleotides and compare the diffusion coefficients extracted by either Fourier analysis or Gaussian fitting of the recorded image. Figures complementary to Figures 3 and 5 and to Table 4. This material is available free of charge via the Internet at http://pubs.acs.org.